

STRUCTURAL AND ELECTRICAL PROPERTIES OF $\text{Ba}(\text{Fe}_{0.5}\text{Nb}_{0.5})\text{O}_3$ - BaTiO_3 CERAMIC SYSTEM

1. SHASHI PRAKASH RAI AND 2. B.K MISHARA

1.Mansa Pandey Bag, Ara – 802301 , Bihar , India

2. Shreenath Niketan , Hazaribagh-825301 , Jharkhand , India

Abstract

Polycrystalline samples of $\text{BaFe}_{0.5}\text{Nb}_{0.5}\text{O}_3$ and $(1-x)\text{Ba}(\text{Fe}_{0.5}\text{Nb}_{0.5})\text{O}_3$ - $x\text{BaTiO}_3$, [referred as BFN and BFN-BT respectively] ($x = 0.00, 0.15$ and 0.20) have been synthesized by a high-temperature solid-state reaction technique. The formation of the compound was checked by an X-ray diffraction (XRD) technique. The microstructure analysis was done by scanning electron micrograph. The spectroscopic data presented in impedance plane show the grain and grain boundary contributions towards electrical processes in the form of semi-circular arcs. Detailed studies of dielectric and impedance properties of the materials in a wide range of frequency (100Hz – 5MHz) and temperatures (30 - 282°C) showed that these properties are strongly temperature and frequency dependent.

Keywords: Dielectric properties; electrical properties; x-ray diffraction; scanning electron micrographs

Introduction

Perovskite-type (ABO_3 type, ($A =$ mono-divalent, $B =$ trid to hexavalent) oxides have attracted a considerable attention of researchers in view of their excellent physical properties such as colossal magnetoresistance, ferroelectric, piezoelectric, magnetoelectric and electro-optic effects, making them suitable for industrial applications [1–5]. The alternating current impedance spectroscopy (ACIS) is a very convenient and powerful experimental technique that enables us to correlate the electrical properties of a material with its microstructure, and also helps to analyze and separate the contributions, from various components (i.e., through grains, grain boundary, interfaces, etc.) of polycrystalline materials in the wide frequency range. The relaxor ferroelectric materials exhibit a large range of interesting properties

related to their complex order/disorder nanostructures. Most relaxor ferroelectrics belong to family of complex lead-based perovskite oxides, such as $\text{Pb}(\text{Mg}_{1/3}\text{Nb}_{2/3})\text{O}_3$ (PMN), which is often considered as a model system. These materials have a disadvantage due to toxicity and volatility of polluting substances. Researchers are directed towards more environmentally friendly lead-free relaxor materials. In this way, many compositions with perovskite structure were recently prepared and characterized [6–20].

Recently giant dielectric constant and dielectric relaxation in $\text{A}(\text{Fe}_{1/2}\text{B}_{1/2}\text{O}_3)$, (A = Ba, Sr and B = Nb, Ta) [21], $\text{CaCu}_3\text{Ti}_4\text{O}_{12}$ [22], CdCr_2S_4 [23] have been pursued to understand the relaxation mechanism, which describes the dielectric relaxation i.e. charge redistribution, structural frustration or polaron redistribution, ferroelectric relaxor, and Maxwell-Wagner space charge (pseudo relaxor)[24].

The relaxor ferroelectric $(1-x)\text{BaFe}_{1/2}\text{Nb}_{1/2}\text{O}_3-x\text{BaTiO}_3$ known as BFN-BT, are the active element in a wide range of piezoelectric devices such as sensors and actuators, ultrasound technologies and under water acoustics. When properly oriented, they have piezoelectric coefficients which are the highest yet reported, with electromechanical deformations one order of magnitude larger than those of conventional high piezoelectric $\text{PbZrO}_3\text{-PbTiO}_3$ (PZT) ceramics [25, 26]. For instant, several researcher, such Intatha et al. [24], Fang et al. [27], Nedelcu et al.[28], Yokosuka [29], Tezuka et al. [30], Raevski et al. [31] and Saha and Sinha [32, 33] have reported that the BFN-based electroceramics exhibit a relaxor behavior by showing very attractive dielectric and electric properties over a wide range of temperatures. However, there still exit considerable debates concerning the physical mechanisms governing their electrical behavior [31]. To our best knowledge, impedance studies of BFN and its perovskite solid solution $(1-x)\text{Ba}(\text{Fe}_{0.5}\text{Nb}_{0.5})\text{O}_3-x\text{BaTiO}_3$, where $x = 0.15, 0.20$, ceramic have not been reported so far. This has prompted us to examine the impedance spectroscopic properties of it with aim of achieving better understanding of their structural, dielectric and electrical behavior of the synthesized ceramics.

Experimental

The polycrystalline samples of $((1-x)\text{Ba}(\text{Fe}_{0.5}\text{Nb}_{0.5})\text{O}_3-x\text{BaTiO}_3$, ($x = 0.00, 0.15, 0.20$) respectively) were prepared from high purity BaCO_3 (99.8% M/S Burgoyne Buirbridger, India), Fe_2O_3 (99.9% M/S Indian rare earth Ltd.) TiO_2 (99.8% M/S John Baker Inc., USA), and Nb_2O_5 (99.9% M/s. Loba Chemie Pvt. Ltd., India) using a high-temperature solid-state

reaction technique. These materials were taken in a suitable stoichiometry ratio and mixed thoroughly with acetone in an agate-mortar for ~ 4 h and dried by slow evaporation method. After that, the mixtures of ingredients of powder was calcined in an alumina crucible at 1200°C for ~ 8 h in air atmosphere. The calcined fine powder was cold pressed into cylindrical pellets of size 10mm of diameter and 1- 2mm of thickness using a hydraulic press with a pressure of 5×10^7 N/m². These pellets were sintered at 1250 °C for 5 h in closed Alumina Crucibles. The formation and quality of compounds were checked by XRD technique. The room temperature (~30°C) X-ray diffraction patterns of the above mentioned compound were recorded using an X-ray powder diffractometer (Rigaku Miniflex, Japan) using CuK_α radiation ($\lambda = 1.5418 \text{ \AA}$) in a wide range of Bragg angles 2θ ($20^\circ \leq 2\theta \leq 80^\circ$) with scanning rate $2^\circ/\text{min}$.

The surface morphology of the gold sputtered samples were recorded with different magnifications at room temperature using a JEOL-JSM-5800 scanning electron micrograph (SEM). The flat polished surface of sintered pellets were electroded with air drying silver paste and fired at 150°C for 2h before taking any electrical measurement. The dielectric constants (ϵ') and loss tangents ($\tan\delta$) of samples were measured as a function of frequency at different temperature (30-282°C) at different frequencies using an impedance analyzer (PSM 1735) while heating at the rate of $0.5^\circ \text{ C min}^{-1}$ with a laboratory-made three-terminal sample holder.

Results and discussion

The sharp and single diffraction peaks of $((1-x)\text{Ba}(\text{Fe}_{0.5}\text{Nb}_{0.5})\text{O}_3-x\text{BaTiO}_3$, ($x = 0.00, 0.15, 0.20$) compounds indicate homogeneity and better crystallization of the samples. The room temperature XRD patterns of the compounds are plot in **Fig 1**. The X-ray analysis indicates that the compounds were of monoclinic structure at room temperature. All the reflection peaks were indexed using observed inter-planar spacing d , and lattice parameters of were determined using a least-squares refinement method. All the calculations were done using standard computer program POWDMULT [34]. A good agreement between calculated and observed d values (**Table 1**) of all diffraction lines (reflections) for $x = 0.00, 0.15$ and 0.20 , suggests that there is no change in the basic crystal structure of system. Our results are in agreement with those by Rama et al. [35] and Tezuka et al. [30], who also prepared this

compound by solid-state reaction. However, Saha and Sinha [32-33] deduced BFN having a monoclinic structure. The lattice parameters of the compounds are given in **Table 2**.

The surface micrographs of $((1-x)\text{Ba}(\text{Fe}_{0.5}\text{Nb}_{0.5})\text{O}_3-x\text{BaTiO}_3$, ($x = 0.00, 0.15, 0.20$) compounds are shown in **Fig. 2**. The nature of the micrographs exhibits the polycrystalline texture of the material having highly distinctive and compact rectangular/cubical grain distributions (with fewer voids). The grain size of A, B and C compounds was found to be in the range of 0.2 -2.8 μm .

The frequency dependence of the dielectric constant (ϵ') of $((1-x)\text{Ba}(\text{Fe}_{0.5}\text{Nb}_{0.5})\text{O}_3-x\text{BaTiO}_3$, ($x = 0.00, 0.15, 0.20$) ceramics at 30°C and 130°C are plotted in **Fig. 3**. At 30°C and 130°C, the dielectric constant (ϵ') has a maximum value of 340 and 940 for $x = 0.00$, 3014 and 7295 for $x = 0.15$, 1908 and 2117 for $x = 0.20$ at 100 Hz. The nature of dielectric permittivity related to free dipoles oscillating in an alternating field may be described in the following way. At very low frequencies ($\omega \ll 1/\tau$, τ is the relaxation time), dipoles follow the field and $\epsilon' \approx \epsilon_s$ (value of the dielectric constant at quasi-static field). As the frequency increases (with $\omega < 1/\tau$), dipoles begin to lag behind the field and ϵ' slightly decreases. When frequency reaches the characteristic frequency ($\omega = 1/\tau$), the dielectric constant drops (relaxation process). At very high frequencies ($\omega \gg 1/\tau$), dipoles can no longer follow the field and $\epsilon' \approx \epsilon_\infty$ (high-frequency value of ϵ') [36]. This behavior is also found in other compounds studied by us [37-41].

Fig. 4 shows the variation of tangent loss ($\tan\delta$) with frequency at 30°C and 130°C. It was observed that the values of the $\tan\delta$ of $x = 0.00$ ceramic decrease with increasing frequency indicating a normal behavior of dielectrics/ferroelectrics. But for $x = 0.15$ and 0.20 ceramics, the nature of variation shows the existence of $\tan\delta$ peak at a particular frequency for a temperature. At low frequencies ($\leq 100\text{Hz}$) and at temperature 130°C, the value of $\tan\delta$ for $x = 0.00$ decreases with increase in frequency for up to a certain frequency value, but for $x = 0.15$ and 0.20 ceramics, it rises to new peak at much higher frequency. But at lower temperature $\tan\delta$ has smaller value which increases on increasing peak position at a certain frequency.

The variation of dielectric constant (ϵ') of $((1-x)\text{Ba}(\text{Fe}_{0.5}\text{Nb}_{0.5})\text{O}_3-x\text{BaTiO}_3$, ($x = 0.00, 0.15, 0.20$) ceramics as a function of temperature at few selected frequencies is shown in **Fig. 5**. In the low-temperature region, ($< 150^\circ\text{C}$), ϵ' is almost constant up to a certain temperature

($\sim 60^\circ\text{C}$ for $x = 0.00$, $\sim 70^\circ\text{C}$ for $x = 0.15$ and $\sim 125^\circ\text{C}$ for $x = 0.20$) and then increases faster up to a 282°C . The variation of tangent loss ($\tan\delta$) as a function of temperature at 1.09 kHz and 2.26 kHz frequencies for $x = 0.00$, 0.15 and 0.20 ceramics are shown in **Fig. 6**. It is observed that, $\tan\delta$ remains almost constant up to 215°C , afterwards, it increases rapidly.

Complex plane impedance plots of $((1-x)\text{Ba}(\text{Fe}_{0.5}\text{Nb}_{0.5})\text{O}_3-x\text{BaTiO}_3$, ($x = 0.00, 0.15, 0.20$) compounds plotting the imaginary part Z'' against the real part Z' of the complex impedance Z^* at temperature 240°C is shown in **Fig. 7(a-c)**. For $x = 0.00, 0.15$ and 0.20 compounds, a single semicircular arc was observed in the complex plane, and this can be explained by a RC equivalent circuit (**Fig. 7a** inset). Generally, the impedance properties of materials arise due to intragrain, intergrain and electrode processes. The motion of charges could occur in a number of ways: (i) dipole reorientation, (ii) space charge formalism and (iii) charge displacement. Thus, the complex impedance formalism allows for a direct separation of the bulk, grain boundary and the electrode phenomena. Complex impedance (Cole–Cole plot) shows polydispersive nature of dielectric phenomena with the possibility of distributed relaxation time as indicated by the semicircular arc at different temperatures with their center located below the real x-axis. For a bulk crystal containing interfacial boundary layer (grain-boundary), the equivalent circuit may be considered as two parallel RC elements connected in series (inset of Fig.) and gives rise to two arcs in complex plane, one for bulk crystal (grain) and the other for the interfacial boundary (grain-boundary) response [**33,41**].

The resistance was obtained from the intersection of the semicircle and the Z' -axis. It was indicating the presence of relaxation species and non-Deby type of relaxation process occurs in the materials.

Fig. 8 shows the ac conductivity of the $((1-x)\text{Ba}(\text{Fe}_{0.5}\text{Nb}_{0.5})\text{O}_3-x\text{BaTiO}_3$, ($x = 0.00, 0.15, 0.20$) samples as a function of frequency at several temperatures between 120°C and 270°C . The ac conductivity of the system depends on the dielectric properties and sample capacitance of the material. In $x = 0.00$ ceramics, presence of both the high and low frequency plateaus in conductivity spectra suggests that the two processes are contributing to the bulk conduction behavior. One of these processes relaxes in the higher frequency region and contribution of the other process appears as a plateau in the higher frequency region. The conductivity shows dispersion which shifts to higher frequency side with the increase of

temperature. The strong frequency dependent conductivity has been found above 10 kHz for $x = 0.15$ and 0.20 which is a typical feature of perovskite at elevated temperature ($>180^{\circ}\text{C}$).

The logarithmic angular frequency dependence of Z' and Z'' of $((1-x)\text{Ba}(\text{Fe}_{0.5}\text{Nb}_{0.5})\text{O}_3-x\text{BaTiO}_3$, ($x = 0.00, 0.15, 0.20$) at several temperatures between 120°C and 270°C is plotted in **Fig. 9** and **Fig. 10** respectively. Z' decreases monotonically with increasing frequency up to certain frequency and then becomes frequency independent at lower temperature. At higher temperatures, Z' is almost constant and for even higher frequencies decreases sharply. As the temperature increases, the peak of Z'' appear for $x = 0.15$ and 0.20 . The peak shifts towards higher frequency with increasing temperature showing that the resistance of the bulk material is decreasing. Also, the magnitude of Z'' decreases with increasing frequencies. This would imply that relaxation is temperature dependent, and there is apparently not a single relaxation time. There by relaxation processes involved with their own discrete relaxation time depending on the temperature. It is evident that with increasing temperature, there is a broadening of the peaks and at higher temperatures, the curves appear almost flat.

Conclusions

Finally, it can be concluded that the polycrystalline samples of $((1-x)\text{Ba}(\text{Fe}_{0.5}\text{Nb}_{0.5})\text{O}_3-x\text{BaTiO}_3$, ($x = 0.00, 0.15, 0.20$) have confirmed the formation of the single phase new compound at room temperature. Sintered pellets were investigated for its dielectric (ϵ' and $\tan\delta$) properties in the temperature range of 30°C - 282°C and in the frequency range of 173 Hz - 5 MHz . Studies of the dielectric constant (ϵ') and tangent loss ($\tan\delta$) of compounds suggested that the higher value of ϵ' at the low frequency region has been explained using Maxwell–Wagner polarization effect. This is associated with heterogeneous conduction in the grains and grain boundaries of the compounds.

References:

1. Ahn, C.H.; Triscone, J. M.; Mannhart, J. *Nature* (London), **2003**, 424, 1015.

DOI:10.1038/nature01878

2. Auciello, O.; Scott, J. F.; Ramesh, R. *Phys. Today*, **1998**, 51, 22.
DOI: 10.1063/1.882324
3. Dorr, K. *J. Phys. D*, **2006**, 39, R125.
DOI: [10.1088/0022-3727/39/7/R01](https://doi.org/10.1088/0022-3727/39/7/R01)
4. Mbenkum, B.N.; Ashkenov, N.; Schubert, M.; Lorenz, M.; Hochmuth, H.; Michel, D.; Grundmann, M.; Wagner, G. *Appl. Phys. Lett.*, **2005**, 86, 091904.
DOI: 10.1063/1.1862778
5. Himanshu, A. K.; Choudhary, B.K.; Gupta, D.C.; Bandyopadhyay, S.K.; Sinha, T.P. *Physica B*, **2010**, 405, 1608–1614.
DOI: [10.1016/j.physb.2009.12.051](https://doi.org/10.1016/j.physb.2009.12.051)
6. Ravez, J.; Simon, A. *J. Korean Phys. Soc.*, **1998**, 32, S955.
DOI: [10.3938/jkps.32.955](https://doi.org/10.3938/jkps.32.955)
7. Ravez, J.; Broustera, C.; Simon, A. *J. Mater. Chem.*, **1999**, 9, 1609.
DOI: 10.1039/A902335F
8. Ravez, J.; Simon, A. *Solid State Sci.*, **2000**, 2, 525.
DOI: [10.1016/S1293-2558\(00\)01066-9](https://doi.org/10.1016/S1293-2558(00)01066-9),
9. Kerfah, A.; Taïbi, K.; Guehria-Laïdoudi, A.; Simon, A.; Ravez, J. *Mater. Lett.*, **2000**, 42, 189.
DOI: [10.1016/S0167-577X\(99\)00182-2](https://doi.org/10.1016/S0167-577X(99)00182-2),
10. Khemakhem, H.; Simon, A.; Vonder Mühl, R.; Ravez, J. *J. Phys.: Condens. Matter*, **2000**, 12, 5951.
DOI: [10.1088/0953-8984/12/27/313](https://doi.org/10.1088/0953-8984/12/27/313)
11. Ravez, J.; Simon, A. *Phys. Status Solidi A*, **2000**, 178, 793.
DOI: 10.1002/1521-396X(200004)178:2<793::AID-PSSA793>3.0.CO;2-X
12. Zhou, L.; Vilarinhoand, P.M.; Baptista, J. L. *J. Electrochem.*, **2000**, 5, 191.
DOI: 10.1023/A:1026586226361
13. Zhou, L.; Vilarinhoand, P.M.; Baptista, J.L. *J. Eur. Ceram. Soc.*, **2001**, 21, 531.
DOI: [10.1016/S0955-2219\(00\)00239-9](https://doi.org/10.1016/S0955-2219(00)00239-9),
14. Bahri, F.; Simon, A.; Khemakhem, H.; Ravez, J. *Phys. Status Solidi A*, **2001**, 184, 459.
DOI: 10.1002/1521-396X(200104)184:2<459::AID-PSSA459>3.0.CO;2-0
15. Ravez, J.; Simon, A. *J. Solid State Chem.*, **2001**, 162, 260.

DOI:[10.1006/jssc.2001.9285](https://doi.org/10.1006/jssc.2001.9285),

16. Komine, S.; Iguchi, E. *J. Phys.: Condens. Matter*, **2002**, 14, 2043.

DOI:[10.1088/0953-8984/14/8/330](https://doi.org/10.1088/0953-8984/14/8/330)

17. Bahri, F.; Khemakhem, H.; Simon, A.; Von der Mühl, R.; Ravez, J. *Solid State Sci.*, **2003**, 5, 1235.

DOI: [10.1016/S1293-2558\(03\)00180-8](https://doi.org/10.1016/S1293-2558(03)00180-8),

18. Simon, A.; Ravez, J. *Solid State Sci.*, **2004**, 5, 1459.

DOI:[10.1016/S1293-2558\(03\)00194-8](https://doi.org/10.1016/S1293-2558(03)00194-8),

19. Salak, A.N.; Shvartsman, V.V.; Seabra, M.P.; Kholkin, A.L.; Ferrera, V.M. *J. Phys.: Condens. Matter*, **2004**, 16, 2785.

DOI:[10.1088/0953-8984/16/16/003](https://doi.org/10.1088/0953-8984/16/16/003)

20. Badapanda, T.; Rout, S.K.; Panigrahi, S.; Sinha, T.P. *Current Applied Physics*, 2009, 9, 727–731.

DOI:[10.1016/j.cap.2008.06.014](https://doi.org/10.1016/j.cap.2008.06.014)

21. Rivera, Kumar, A.; Ortega, N.; Katiyar, R. S.; Lushnikov, S. *Sol. State Comm.*, **2009**, 149, 172.

DOI:[10.1016/j.ssc.2008.10.026](https://doi.org/10.1016/j.ssc.2008.10.026)

22. Sinclair, D. C.; Adams, T. B.; Morrison, F. D.; West, A. R. *Appl. Phys Lett.*, **2002**, 80, 2153.

DOI: [10.1063/1.1463211](https://doi.org/10.1063/1.1463211)

23. Catalan, G. *Appl. Phys. Lett.*, **2006**, 88, 102902.

DOI: [10.1063/1.2177543](https://doi.org/10.1063/1.2177543)

24. Intatha, U.; Eitssayeam, S.; Wang, J.; Tunkasiri; *Curr. Appl. Phys.*, **2010**, 10, 21-25.

DOI: [10.1016/j.cap.2009.04.006](https://doi.org/10.1016/j.cap.2009.04.006),

25. Park S. E.; Shrout, T. R. *J. Appl. Phys.*, **1997**, 82, 1804.

DOI: [10.1063/1.365983](https://doi.org/10.1063/1.365983)

26. Viehland, D.; Amin, A.; Li, J. F. *Appl. Phys. Lett.*, **2001**, 79, 1006.

DOI: [10.1063/1.1392307](https://doi.org/10.1063/1.1392307)

27. Fang, B.; Cheng, Z.; Sun, R.; Ding, C. *J. Alloys Compd.*, 2009, 471, 539-543.

DOI: [10.1016/j.jallcom.2008.04.056](https://doi.org/10.1016/j.jallcom.2008.04.056)

28. Nedelcu, L.; Toacsan, M.I.; Banciu, M.G.; Ioachim, A. *J. Alloys Compd.*, **2011**, 509, 477-481.
DOI:[10.1016/j.jallcom.2010.09.069](https://doi.org/10.1016/j.jallcom.2010.09.069)
29. Yokosuka, M. *Jpn. J. Appl. Phys.*, **1995**, 34, 5338.
DOI: 10.1143/JJAP.34.5338
30. Tezuka, K.; Henimi, K.; Hinatsu, Y.; Masaki, N. M. *J. Solid State Chem.*, **2000**, 154, 591.
DOI: [10.1006/jssc.2000.8900](https://doi.org/10.1006/jssc.2000.8900)
31. Raevski, I. P.; Prosandeev, S. A.; Bogatin, A. S.; Malitskaya, M.A.; Jastrabik, L. *J. Appl. Phys.*, **2003**, 93, 4130.
DOI:[10.1063/1.1558205](https://doi.org/10.1063/1.1558205)
32. Saha, S.; Sinha, T. P. *J. Phys.: Condens. Matt.*, **2002**, 14, 249.
DOI:[10.1088/0953-8984/14/2/311](https://doi.org/10.1088/0953-8984/14/2/311)
33. Saha, S.; Sinha, T.P. *Phys. Rev. B*, **2002**, 65, 134103.
DOI:[10.1103/PhysRevB.65.134103](https://doi.org/10.1103/PhysRevB.65.134103)
34. E. Wul, PowdMult, An interactive powder diffraction data interpretation and index program, version 2.1, school of Physical science, Flinders University of South Australia, Bedford Park, S.A. 5042, Australia.
35. Rama, N.; Philipp, J.B.; Opel, M.; Chandrasekaran, K.; Sankaranarayanan, V.; Gross, R.; Rao, M.S.R. *J. Appl. Phys.* 2004, 95, 7528.
DOI: [10.1063/1.1682952](https://doi.org/10.1063/1.1682952)
36. Himanshu, A.K.; Bandyopadhyay, S.K.; Sen, P.; Mondal, N. N.; Talpatra, A.; Taki, G.S.; Sinha, T.P. *Rad. Phys Chem.*, **2010**, 80, 414-419.
DOI:[10.1016/j.radphyschem.2010.09.007](https://doi.org/10.1016/j.radphyschem.2010.09.007)
37. Singh, N.K.; Kumar, P.; Kumar, H.; Rai, R. *Adv. Mat. Lett.* **2010**, 1, 79-82.
DOI: 10.5185/amlett.2010.3102
38. Singh, N.K.; Roy, O.P.; Rai, R. *J. Alloys Compd.*, **2010**, 507, 542-546.
DOI:[10.1016/j.jallcom.2010.08.015](https://doi.org/10.1016/j.jallcom.2010.08.015)
39. Singh, N.K.; Choudhary, R. N. P.; Banarji, B. *Physica B*, **2008**, 403, 1673.
DOI: [10.1016/j.physb.2007.09.083](https://doi.org/10.1016/j.physb.2007.09.083),
40. Kumar, P.; Singh, B.P.; Sinha, T.P.; Singh, N.K. *Physica B*, **2011**, 406, 139–143.

DOI: [10.1016/j.physb.2010.09.019](https://doi.org/10.1016/j.physb.2010.09.019)

41. Singh, N.K.; Kumar, P.; Kumar, H.; Rai, R. *Adv. Mat. Lett.* **2011**, 2, 200-205.

DOI: [10.5185/amlett.2010.11178](https://doi.org/10.5185/amlett.2010.11178)

Figure Captions

Fig. 1 X-ray diffraction pattern of $((1-x)\text{Ba}(\text{Fe}_{0.5}\text{Nb}_{0.5})\text{O}_3-x\text{BaTiO}_3$, ($x = 0.00, 0.15, 0.20$) compounds.

Fig. 2 SEM-micrographs of $((1-x)\text{Ba}(\text{Fe}_{0.5}\text{Nb}_{0.5})\text{O}_3-x\text{BaTiO}_3$, ($x = 0.00$ (A), 0.15 (B), 0.20 (C)) compounds at room temperature.

Fig. 3 Frequency dependence of dielectric constant (ϵ') of $((1-x)\text{Ba}(\text{Fe}_{0.5}\text{Nb}_{0.5})\text{O}_3-x\text{BaTiO}_3$, ($x = 0.00, 0.15, 0.20$) compounds at 30°C and 130°C .

Fig. 4 Frequency dependence of tangent loss ($\tan\delta$) of $((1-x)\text{Ba}(\text{Fe}_{0.5}\text{Nb}_{0.5})\text{O}_3-x\text{BaTiO}_3$, ($x = 0.00, 0.15, 0.20$) compounds at 30°C and 130°C .

Fig. 5 Variation of dielectric constant (ϵ') with temperature of $((1-x)\text{Ba}(\text{Fe}_{0.5}\text{Nb}_{0.5})\text{O}_3-x\text{BaTiO}_3$, ($x = 0.00, 0.15, 0.20$) compounds at 1.09 kHz and 2.26 kHz.

Fig. 6 Variation of tangent loss ($\tan\delta$) with temperature of $((1-x)\text{Ba}(\text{Fe}_{0.5}\text{Nb}_{0.5})\text{O}_3-x\text{BaTiO}_3$, ($x = 0.00, 0.15, 0.20$) compounds at 1.09 kHz and 2.26 kHz.

Fig. 7 Complex plane impedance plot of $((1-x)\text{Ba}(\text{Fe}_{0.5}\text{Nb}_{0.5})\text{O}_3-x\text{BaTiO}_3$, ($x = 0.00, 0.15, 0.20$) at 240°C and RC equivalent circuit (inset).

Fig. 8 Variation of σ_{ac} with angular frequency for $((1-x)\text{Ba}(\text{Fe}_{0.5}\text{Nb}_{0.5})\text{O}_3-x\text{BaTiO}_3$, ($x = 0.00, 0.15$ and 0.20) at various temperatures.

Fig.9 Variation of Z' with angular frequency for $((1-x)\text{Ba}(\text{Fe}_{0.5}\text{Nb}_{0.5})\text{O}_3-x\text{BaTiO}_3$, ($x = 0.00, 0.15$ and 0.20) at various temperatures.

Fig.10 Variation of Z'' with angular frequency for $((1-x)\text{Ba}(\text{Fe}_{0.5}\text{Nb}_{0.5})\text{O}_3-x\text{BaTiO}_3$, ($x = 0.00, 0.15$ and 0.20) at various temperatures.

Table 1. Comparison of observed (obs) and calculated (cal) d-values (in Å) of some reflections of $((1-x)\text{Ba}(\text{Fe}_{0.5}\text{Nb}_{0.5})\text{O}_3-x\text{BaTiO}_3$, ($x = 0.00, 0.15, 0.20$) compounds at room temperature with intensity ratio I/I_0 .

(hkl)	x = 0.00	x = 0.15	x = 0.20
	d (Å)	d (Å)	d (Å)
(100)	[o] 4.0337 (17)	[o] 4.0295 (69)	[o] 4.0187 (81)

	[c] 4.0337	[c] 4.0295	[c] 4.0187
(001)	[o] 2.8553 (100)	[o] 2.8625 (100)	[o] 2.8544 (100)
	[c] 2.8553	[c] 2.8625	[c] 2.8544
(101)	[o] 2.3329 (43)	[o] 2.3369 (78)	[o] 2.3250 (88)
	[c] 2.3283	[c] 2.3287	[c] 2.3293
(111)	[o] 2.0213 (55)	[o] 2.0247 (85)	[o] 2.0179 (92)
	[c] 2.0213	[c] 2.0184	[c] 2.0151
(210)	[o] 1.8181 (26)	[o] 1.8020 (72)	[o] 1.7957 (85)
	[c] 1.8226	[c] 1.8036	[c] 1.7991
(201)	[o] 1.6581 (66)	[o] 1.6537 (93)	[o] 1.6518 (99)
	[c] 1.6537	[c] 1.6441	[c] 1.6416
(220)	[o] 1.4331 (56)	[o] 1.4250 (86)	[o] 1.4238 (89)
	[c] 1.4331	[c] 1.4276	[c] 1.4245
($\bar{1}02$)	[o] 1.3578 (30)	[o] 1.3452 (83)	[o] 1.3439 (85)
	[c] 1.3573	[c] 1.3468	[c] 1.3441
(221)	[o] 1.2816 (52)	[o] 1.2781 (73)	[o] 1.2714 (89)
	[c] 1.2800	[c] 1.2760	[c] 1.2739
(301)	[o] 1.2175(29)	[o] 1.2140 (76)	[o] 1.2122 (84)
	[c] 1.2154	[c] 1.2139	[c] 1.2118

Table 2: Structural data for $((1-x)\text{Ba}(\text{Fe}_{0.5}\text{Nb}_{0.5})\text{O}_3-x\text{BaTiO}_3$, ($x = 0.00, 0.15, 0.20$) compounds.

Sample	Structure	a (Å)	b (Å)	c (Å)	β (in degree)	V
x = 0.00	Monoclinic	4.0337	4.0734	2.8553	90.12	46.92

x = 0.15	Monoclinic	4.0296	4.0465	2.8625	90.25	46.67
x = 0.20	Monoclinic	4.0188	4.0396	2.8544	91.11	46.34

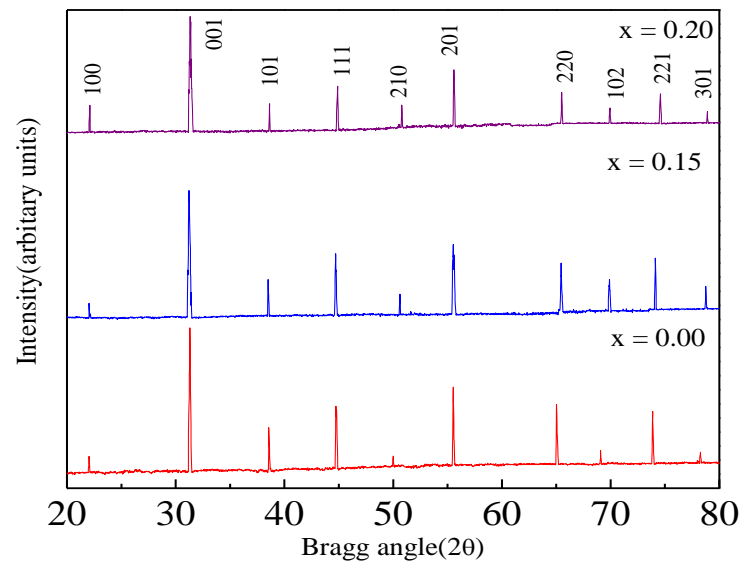
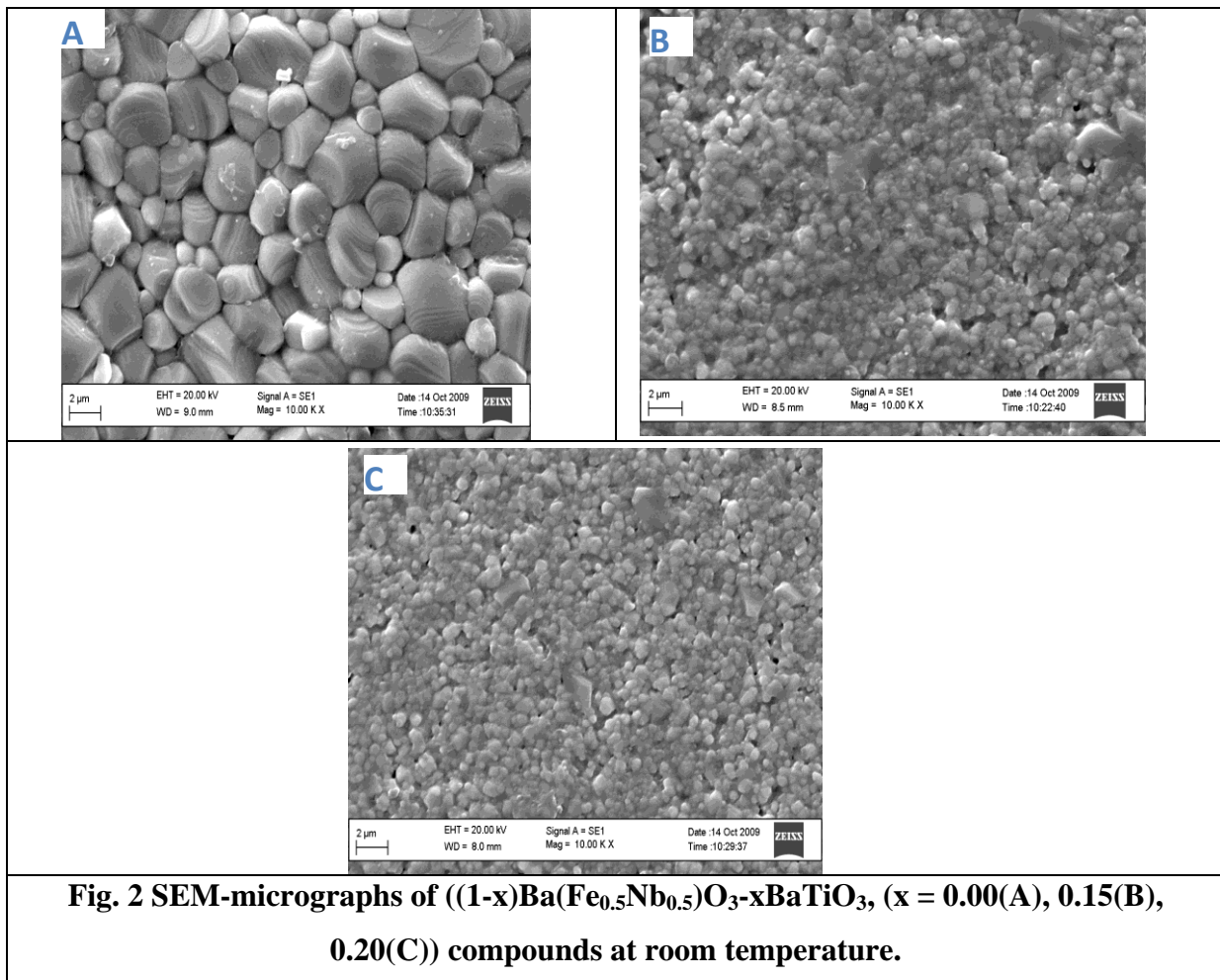


Fig. 1 X-ray diffraction pattern of $((1-x)\text{Ba}(\text{Fe}_{0.5}\text{Nb}_{0.5})\text{O}_3-x\text{BaTiO}_3)$, ($x = 0.00, 0.15, 0.20$) compounds.



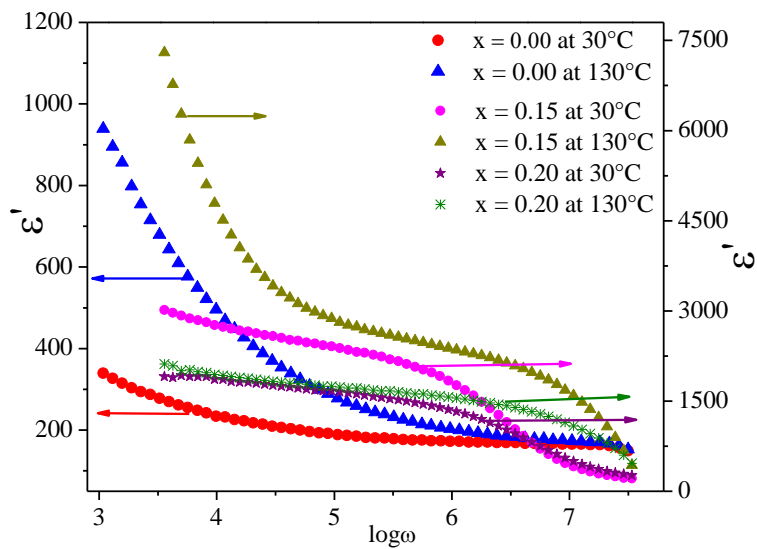


Fig. 3 Frequency dependence of dielectric constant (ϵ') of $((1-x)\text{Ba}(\text{Fe}_{0.5}\text{Nb}_{0.5})\text{O}_3-x\text{BaTiO}_3$, ($x = 0.00, 0.15, 0.20$) compounds at 30°C and 130°C .

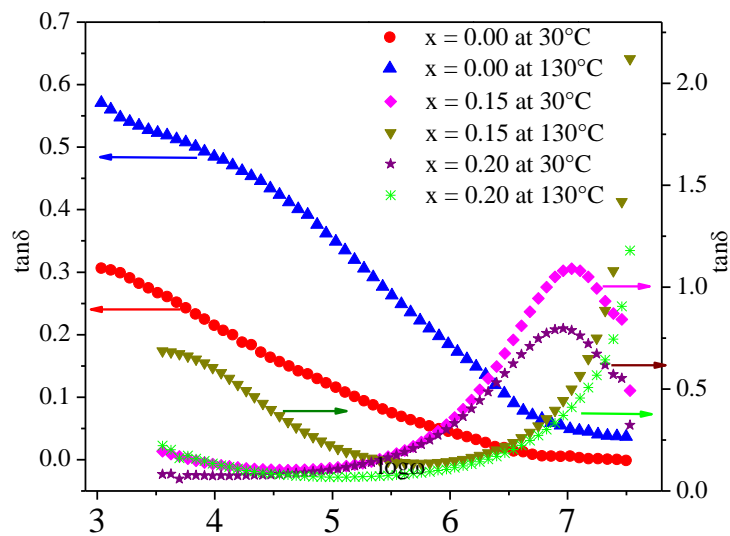


Fig. 4 Frequency dependence of tangent loss ($\tan\delta$) of $((1-x)\text{Ba}(\text{Fe}_{0.5}\text{Nb}_{0.5})\text{O}_3-x\text{BaTiO}_3$, ($x = 0.00, 0.15, 0.20$) compounds at 30°C and 130°C .

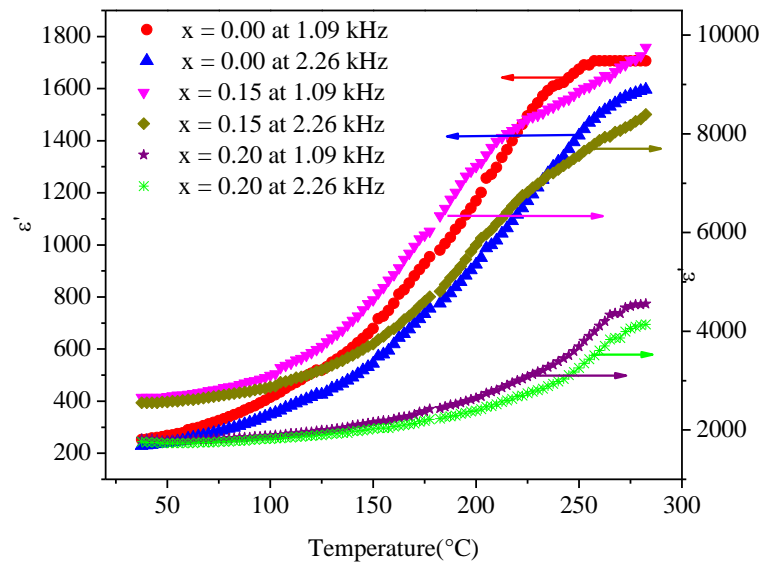


Fig. 5 Variation of dielectric constant (ϵ') with temperature of $((1-x)\text{Ba}(\text{Fe}_{0.5}\text{Nb}_{0.5})\text{O}_3-x\text{BaTiO}_3$, ($x = 0.00, 0.15, 0.20$) compounds at 1.09 kHz and 2.26 kHz.

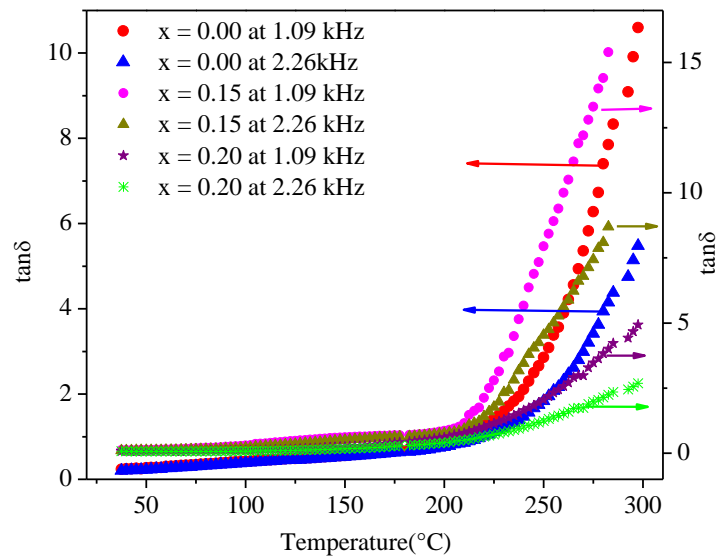


Fig. 6 Variation of tangent loss ($\tan\delta$) with temperature of $((1-x)\text{Ba}(\text{Fe}_{0.5}\text{Nb}_{0.5})\text{O}_3-x\text{BaTiO}_3$, ($x = 0.00, 0.15, 0.20$) compounds at 1.09 kHz and 2.26 kHz.

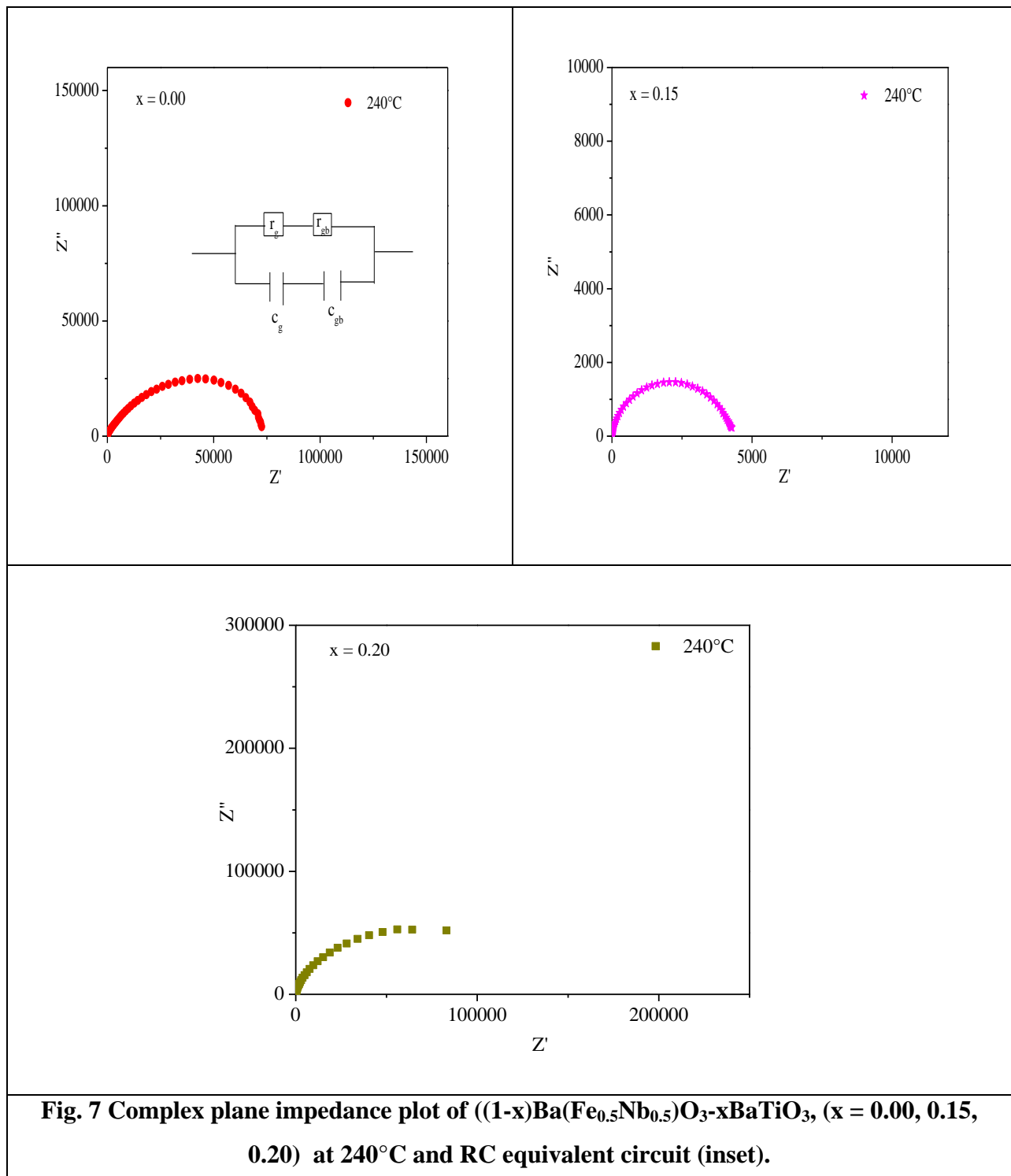


Fig. 7 Complex plane impedance plot of $((1-x)\text{Ba}(\text{Fe}_{0.5}\text{Nb}_{0.5})\text{O}_3-x\text{BaTiO}_3$, ($x = 0.00, 0.15, 0.20$) at 240°C and RC equivalent circuit (inset).

